Title: Distal axotomy enhances retrograde presynaptic excitability onto injured pyramidal neurons via trans-synaptic signaling

Authors: Tharkika Nagendran[1,3], Rylan S. Larsen[2,3,8], Rebecca L. Bigler[5], Shawn B. Frost[6,7], Benjamin D. Philpot[2,3,4], Randolph J. Nudo[6,7], Anne Marion Taylor[1,3,4]*

Affiliations:

[1] UNC/NCSU Joint Department of Biomedical Engineering, UNC-Chapel Hill, Chapel Hill, NC 27599 USA

[2] Department of Cell Biology and Physiology, UNC-Chapel Hill, Chapel Hill, NC 27599 USA

[3] Neuroscience Center, UNC-Chapel Hill, Chapel Hill, NC 27599 USA

[4] Carolina Institute for Developmental Disabilities, Chapel Hill, NC 27599 USA

[5] Curriculum in genetics and Molecular Biology Curriculum, UNC-Chapel Hill, Chapel Hill, NC 27599 USA

[6] Landon Center On Aging, University of Kansas Medical Center, Kansas City, KS 66160 USA

[7] Department of Rehabilitation Medicine, University of Kansas Medical Center, Kansas City, KS 66160 USA

[8]Present address: Allen Institute for Brain Science, Seattle, WA 98109, USA

*To whom correspondence should be addressed: amtaylor@unc.edu

Abstract

Injury of descending motor tracts remodels cortical circuitry and leads to enhanced neuronal excitability, thus influencing recovery following injury. The neuron-specific contributions remain unclear due to the complex cellular composition and connectivity of the CNS. We developed a microfluidics-based *in vitro* model system to examine intrinsic synaptic remodeling following axon damage. We found that distal axotomy of cultured rat pyramidal neurons caused dendritic spine loss at synapses onto the injured neurons followed by a persistent retrograde enhancement in presynaptic excitability over days. These *in vitro* results mirrored hyper-activity of directly injured corticospinal neurons in hindlimb motor cortex layer Vb following spinal cord contusion. *In vitro* axotomy-induced hyper-excitability coincided with elimination of inhibitory presynaptic terminals, including those formed onto dendritic spines. We identified netrin-1 as downregulated following axotomy and exogenous netrin-1 applied 2 days after injury normalized spine density, presynaptic excitability, and the fraction of inhibitory inputs onto injured neurons. These findings demonstrate a novel model system for studying the response of pyramidal circuitry to axotomy and provide new insights of neuron-specific mechanisms that contribute to synaptic remodeling.

Introduction

Acquired brain injuries, such as occur in stroke and traumatic brain injury, induce significant synaptic reorganization, even in uninjured cortical regions remote from the site of damage [1-3]. This enhanced neural plasticity supports formation of new connections and expansion of cortical territories, well-described in humans using neuroimaging and non-invasive stimulation techniques [1, 2, 4, 5]. However, the cellular mechanisms of this injury-induced plasticity remain largely unknown.

In healthy brains, long projection neurons with somatodendritic domains housed in cerebral cortex extend axons into numerous distant areas of the CNS, including the spinal cord and the apposing cortical hemisphere. When these remote areas are injured, long projection axons are damaged and injury signals propagate retrogradely to somatodendritic domains. Retrograde injury signal propagation leads to somatic responses such as chromatolysis and new transcription [6, 7]. For example, after damage to corticospinal axons resulting from spinal cord injury, dendritic spines in motor cortex undergo time-dependent changes in morphology including decreased spine density and alterations in spine length and diameter [8]. Loss of local GABAergic inhibition also occurs at somatodendritic regions following injury, which is thought to unmask preexisting excitatory connections and result in enhanced excitability [2, 9, 10]. These findings suggest that a cascade of events occurs following distal axonal injury involving retrograde axon-to-soma signaling and then trans-synaptic signaling from the injured neuron to uninjured presynaptic neurons causing synaptic changes and enhanced excitability.

Due to the heterogeneity and complexity of the CNS, intrinsic neuronal responses to distal axon injury and neuron-specific contributions to synaptic remodeling remain

unclear. Reduced preparations are valuable for examining these neuron-specific responses and provide a more experimentally tractable model system to identify and screen drugs to improve neuronal function following injury. Because brain injury and disease preferentially affect long projection neurons [11, 12], we sought to determine the progression of events that occur intrinsically in these neurons following distal axotomy leading to trans-synaptic changes.

Results

In vitro model to study distal axon injury to pyramidal neurons

To investigate how distal axon injury remodels synapses contacting injured neurons, we used a microfluidic approach to compartmentalize cultured neurons. Microfluidic chambers containing microgroove-embedded barriers approximately 900 µm in length were used to compartmentalize axons independently from dendrites and somata of rat central neurons as demonstrated previously (**Figure supplement 1a**) [13-15]. Using this approach we subjected neurons to distal axotomy ~1 mm away from their physically undisturbed dendrites and somata as described previously [13, 14]. We used hippocampal neurons harvested from embryonic rats due to the ability to generate a consistent, enriched population of pyramidal neurons (85-90% pyramidal) which exhibit morphology characteristic of maturing pyramidal neurons *in vivo* [16]; the remaining hippocampal neurons are mostly inhibitory GABAergic interneurons [17]. To identify neurons with axons projecting into the axonal compartment, we retrogradely labeled neurons by applying a G-deleted rabies virus expressing fluorescent proteins (incompetent for trans-synaptic transfer) to the axonal compartment and characterized the

morphology of the labeled neurons. We found that 94% (42 of 45) of virally-labeled neurons were pyramidal neurons and the remaining were unclassifiable (**Figure 1a**). When these neurons were cultured within the microfluidic chamber and axotomized within the axonal compartment (**Figure 1b**), the axotomized cultures showed no loss in viability post-axotomy (**Figure supplement 1**), similar to *in vivo* findings [18], and injured axons regrew [13, 14]. Supporting the use of this *in vitro* approach, we previously found that axotomy performed within the microfluidic chambers induced rapid expression of the immediate early gene *c-fos* [13], as reported *in vivo* [19]. Neurons labeled with retrograde tracer, Alexa 568-conjugated cholera toxin, also showed a significant decrease in Nissl staining in the somata reflective of chromatolysis at 24 h post-axotomy [20] (**Figure supplement 1**). Together, this *in vitro* model recapitulated key features of axotomy *in vivo,* and allowed us to examine the response of injured pyramidal neurons far from the site of injury.

Spine density decreases after distal axon injury

Decreased spine density is seen *in vivo* in models of traumatic brain injury and spinal cord injury [21, 22]. To determine whether similar structural changes occur in cultured pyramidal neurons following distal axotomy, we quantified spine density within the somatodendritic compartment of axotomized neurons that were retrogradely labeled using rabies mCherry virus. Spine density significantly declined 24 h and 48 h post-axotomy compared to before axotomy (**Figure 1c,d** and **Figure supplement 2**). In contrast, uninjured control neurons show increased spine density as occurs during normal maturation (**Figure 1c,d)**.

We next analyzed specific spine types that were lost. We found a significant decrease in the density of thin spines at 24 h post-axotomy compared to pre-axotomy (**Figure 2a**). The density of stubby and mushroom spines remained similar before and 24 h after axotomy, unlike in the uninjured control neurons where spine density of all spine types increased. At 48 h post-axotomy the density of both thin and mushroom spines was significantly reduced (**Figure 2a**). The reduction in spine density following axotomy suggests that either dendritic spines were being eliminated or, conversely, that there was a reduction in new spine formation following axotomy. Further analysis of our before and after axotomy images revealed that axotomy caused both a significant increase in the percentage of spines eliminated *and* a significant reduction in the percentage of new spines formed 24 h post-axotomy (**Figure 2b-d**). Thus, axotomy affected both elimination and formation of spines to result in lower dendritic spine density.

A persistent enhancement in synaptic vesicle release rate follows distal injury

To further evaluate how synapses are modified following distal axon injury, we next investigated whether presynaptic release properties were altered at synapses onto injured neurons. To address this question, we retrogradely infected neurons using a modified eGFP rabies virus to label injured neurons and then used FM dyes to optically measure synaptic vesicle release onto these directly-injured neurons (**Figure 3a)**. The use of FM dyes provided us with a non-selective, unbiased method to label a majority of presynaptic terminals within the somatodendritic compartment [23]. FM puncta highly colocalized with synapsin1 immunolabeling (93%), which is present at both inhibitory and excitatory terminals, validating our FM dye loading strategy (**Figure supplement 3**).

We examined the synaptic vesicle release rate of FM puncta that colocalized with axotomized eGFP expressing neurons. At 24 h post-axotomy, there was no change in synaptic vesicle release rate compared to eGFP expressing uninjured control samples (**Figure 3b,c**). In contrast, synaptic vesicle release rate was significantly enhanced 48 h after axotomy (**Figure 3c**). Further, the FM decay time constant, τ, which has been inversely correlated with release probability [24] was significantly reduced at 48 h post-axotomy (control: 138.3 s ± 8.761 versus axotomy: 88.62 s ± 5.132; $p<0.0001$). These results were similar to those obtained by examining the entire image field of FM puncta closest to the barrier region within the somatodendritic compartment where a large percentage of axotomized neurons reside (**Figure supplement 4**). The difference in presynaptic release rate persisted, though modestly, at 4 d post-axotomy in these cultured neurons (control: 88.3 s ± 1.43 versus axotomy: 82.3 s ± 1.552; $p=0.0046$; **Figure supplement 4**). Together, these data suggest a delayed and persistent increase in synaptic vesicle release rate that occured following dendritic spine loss.

Next, we performed two control experiments to determine (1) whether cortical cultures, which have more neuron variaiblity than hippocampal cultures, would behave similarly to hippocampal cultures used in our experimental model, and (2) whether axotomy of axons forming synapses onto postsynaptic targets would yield similar effects on retrograde presynaptic vesicle release as axotomy of untargeted axons. First, we performed the FM unloading experiments with cortical neurons harvested from embryonic rats and found that these cultures showed similar changes in presynaptic release 48 h post-axotomy (**Figure supplement 4**). To address the second question, we added a small number of target neurons to the axonal compartment during cell plating.

153 We previously showed extensive synapse formation when two neuron populations are
154 plated into opposing compartments [15]. Our data show that axotomy to this targeted
155 population of neurons resulted in similar changes in presynaptic release rate as axotomy
156 of untargeted axons (**Figure supplement 4**).

157 We next wondered whether the fraction of responsive to unresponsive presynaptic
158 terminals might be altered following axotomy to allow enhanced excitability even though
159 dendritic spine density is lower. We measured the proportion of FM puncta that unloaded
160 (responsive) or did not unload (unresponsive) in response to field stimulation using
161 extracellular electrodes [23] (**Figure 3d**). At 24 h post-axotomy when spine density was
162 decreased, we observed no change in the fraction of responsive and unresponsive FM
163 puncta compared to uninjured controls (**Figure 3d**). However at 48 h post-axotomy, a
164 significantly larger proportion of puncta were responsive compared to uninjured control
165 chambers (**Figure 3d**). Further, at 48 h post-axotomy we also found an overall decrease
166 in the number of FM puncta, yet the number of responsive FM puncta remained similar to
167 the age-matched control (**Figure 3e**). Together, our data suggest that distal axon injury
168 leads to an overall decrease in quantity of presynaptic terminals, but that this smaller pool
169 of presynaptic terminals is more responsive to stimulation.

170

171 *Enhanced glutamate release occurs at synapses onto injured neurons*

172 Our results support that distal axotomy triggers a retrograde and trans-synaptic
173 cascade of events leading to enhanced neurotransmitter release. To confirm this, we
174 performed electrophysiological recordings of AMPAR-mediated miniature excitatory
175 postsynaptic currents (mEPSCs) from axotomized neurons 48 h post-axotomy and their

age-matched uninjured controls. Biocytin was used to fill neurons following each recording to determine whether neurons extended axons into the axonal compartment and were axotomized. Axotomized neurons had a significant increase in mEPSC frequency, supporting an increased rate of presynaptic glutamate release (**Figure 3f,g**). Membrane properties were equivalent between axotomized and uninjured control neurons, demonstrating that the health of these axotomized neurons was not substantially compromised (**Table supplement 1**). We observed a trend towards an increase in mEPSC amplitude following axotomy, however this effect was not significant (**Figure 3g**).

We next wondered if the increased spontaneous release rate of glutamate was specific to directly injured neurons or more globally affected neighboring, uninjured neurons. To address this, we quantified mEPSC frequency between uncut and cut neurons within the same axotomized chamber. In recordings from directly injured neurons, axotomy specifically increased mEPSC frequency. However, neighboring uninjured neurons that did not extend axons into the axonal compartment, did not have an increased mEPSC frequency (**Figure 3h**). To further examine the effects of direct injury to axotomized neurons, we quantified FM release rate at nearby uninjured neurons that were not infected with the retrograde eGFP rabies virus. We found that the release rate was significantly decreased at these locations compared with synapses on directly axotomized neurons and not significantly different than at control uninjured neurons labeled with eGFP rabies virus (**Figure 3i**). These observations confirmed that axotomy altered glutamatergic synaptic input onto injured neurons. Further, directly injured neurons transynaptically and locally influenced presynaptic glutamate release without affecting

199 nearby synapses at uninjured neurons.

200

201 *Spinal cord injury (SCI) induces persistent and enhanced firing rates in layer Vb*

202 To evaluate the *in vivo* relevance of our findings, we sought to determine whether
203 distal injury of long projection neurons *in vivo* would preferentially induce enhanced
204 excitability in these injured neurons. To do this, we used a rat SCI model described
205 previously [25] in which animals were subjected to a spinal cord contusion injury at
206 thoracic level T9-10, and recording electrodes were implanted into the
207 neurophysiologically-identified hindlimb motor cortex in ketamine-anesthetized animals.
208 Electrode sites on single-shank microelectrode arrays (Neuronexus, Ann Arbor, MI)
209 extended through cortical layers V and VI, allowing simultaneous recording throughout
210 these cortical layers. Effective injury to the corticospinal neurons innervating hindlimb
211 motor neuron pools in the spinal cord was confirmed by stimulating electrode sites and
212 confirming loss of evoked hindlimb movement. At each cortical location, 5 minutes of
213 neural data was collected for offline analysis. At the end of the procedure, neural spikes
214 were discriminated using principle component analysis. We examined firing rates [26]
215 within layers Va, Vb, and VI between 4 weeks and 18 weeks post-SCI and compared the
216 data to sham control animals. We found that the firing rate within layer Vb was
217 significantly increased after SCI compared to sham controls (**Figure 4**). Layer Vb
218 contains the highest density of corticospinal somata, with estimates of nearly 80% of
219 large pyramidal cells [27]. Also, after spinal cord injury, chromatolytic changes occur
220 preferentially in layer Vb [28]. In layers Va and VI, which have few (layer Va) or no (layer
221 VI) corticospinal neurons, we found that firing rates were not statistically different

between SCI animals and sham controls. Together, these data confirm a persistent increase in spontaneous firing rates in remotely injured corticospinal neurons, and support the relevance of our *in vitro* model system.

Axotomy selectively eliminates GABAergic terminals onto spines of injured neurons

Loss of inhibition following distal injury contributes to enhance excitability *in vivo*, thus we wanted to test whether axotomy in our culture system results in a similar loss of inhibitory terminals. We performed retrospective immunostaining to determine the fraction of vGLUT1 or GAD67-positive FM puncta at 48 h post-axotomy (**Figure 5a,b**). We found that axotomy did not alter the fraction of glutamatergic terminals, but significantly diminished the fraction of GAD67-positive puncta within the somatodendritic compartment. Further, we examined the fraction of vGLUT1 or VGAT puncta colocalized with axotomized neurons labeled with eGFP rabies virus 48 h post-axotomy (**Figure 5c**). These results confirmed the preferential absence of inhibitory terminals following axotomy while the fraction of vGLUT1 puncta remained equivalent to uninjured control neurons.

To determine whether inhibitory synapses were functionally altered following axotomy, we recorded miniature inhibitory postsynaptic currents (mIPSCs) from axotomized and uninjured chambers 48h post-axotomy (**Figure 5d-f**). We found that mIPSCs were more frequent in axotomized cultures compared with uninjured neurons, suggesting that while there are fewer inhibitory terminals, the remaining terminals have an increased rate of spontaneous GABA release. We next asked whether this change in inhibitory synapse function was restricted to directly injured neurons. Within the

245 axotomized cultures, we compared both cut and uncut neurons and found that the mIPSC
246 frequency was increased in both groups, but was not different between the directly
247 axotomized neurons and their uncut neighbors. This suggests that the alteration of
248 inhibitory synaptic transmission following axotomy affects both directly injured and
249 neighboring, uninjured neurons.

250 Although the majority of GABAergic synapses are found on dendritic shafts or
251 cell bodies, a minor population is also found on dendritic spines [29, 30] (**Figure**
252 **supplement 6**). Inhibitory synapses formed on dendritic spines allow for
253 compartmentalization of dendritic calcium levels involved in regulation of neuronal
254 activity [31, 32]. To investigate whether dendritic spines receiving inhibitory inputs (i.e.,
255 inhibited spines) are lost following axotomy, we quantified the number of inhibitory and
256 excitatory presynaptic terminals onto spines of cultured pyramidal neurons subjected to
257 distal axotomy compared to uninjured controls using retrospective immunostaining for
258 inhibitory (vGAT) and excitatory (vGLUT1) synapse markers. We found a significant
259 decrease in the fraction of vGAT-positive spines at 48h post-axotomy compared to
260 uninjured control (**Figure 5g-i)** with no significant influence on glutamatergic spines.
261 Together, our data suggest that axotomy caused a preferential loss of inhibitory terminals
262 onto axotomized neurons, including inhibitory terminals formed onto dendritic spines,
263 and that increased spontaneous GABAergic transmission might compensate to some
264 degree for these lost terminals.

265

266

Local activity, retrograde signaling and differential gene expression regulate axotomy induced synaptic changes

Efficient axon regeneration requires signaling from the site of injury to the nucleus in multiple model systems [6], yet the signaling events required for synaptic remodeling following distal axotomy remain unclear. Breach of the axonal membrane following axon injury causes an influx of calcium and sodium ions into the intra-axonal space, potentially influencing signaling to the nucleus and gene expression. To determine whether local influx of sodium and calcium ions at the time of injury is required for axotomy-induced spine loss, we performed axotomy within the axonal compartment in which axons were treated with a local activity blockade during axotomy. This local activity blockade solution (ABS) included low-Ca2+, high-Mg2+, and TTX (0.5 mM CaCl2, 10 mM MgCl2, 1 μM TTX) to prevent influx of sodium and reduce calcium influx. This local activity blockade was applied solely to the axonal compartment for 1 h during axotomy. We labeled neurons extending axons into the axonal compartment using a retrograde eGFP rabies virus and quantified spine density before and 24 h following axotomy and compared these measurements to cultures with vehicle applied to axons during axotomy (**Figure 6a,b**). Strikingly, we found that local activity blockade at the injury site prevented axotomy-induced spine loss. These data suggest that local activity instructs retrograde signaling and spine loss.

To determine whether injury-induced transcription is required for these trans-synaptic changes, we treated the somatodendritic compartment with the reversible transcriptional blocker DRB 15 min prior to axon injury and removed the drug 45 minutes later. We found that blocking transcription during this brief time was sufficient

to prevent axotomy-induced spine loss 24 h post-axotomy compared with similarly treated uninjured control chambers (**Figure 6c**). Further, DRB treatment at the time of injury prevented significant changes in the proportion of responsive FM puncta (**Figure 6d**) and in synaptic vesicle release rate 48 h post-axotomy (**Figure 6e**). However, action potential blockade with TTX in the somatodendritic compartment for ~1 h at the time of injury did not affect injury-induced changes in presynaptic release or the proportion of responsive puncta (**Figure 6g,h**). Further, application of HBS or DMSO as respective vehicle controls to TTX or DRB treatments did not alter injury-induced increase in presynaptic release. We conclude that both local activity at the site of injury and a transcriptional response were critical mediators of the delayed trans-synaptic changes in presynaptic release properties following distal axon injury.

Differential gene expression at 24 h post-axotomy

Our data show that a transcriptional response was required immediately after axotomy to induce retrograde changes in synaptic vesicle release onto injured neurons. To identify genes that might mediate this process within a longer therapeutically-relevant time window, we performed a gene expression study to identify differentially expressed transcripts within the somatodendritic compartment at 24 h post-axotomy compared to uninjured controls. We found 615 transcripts that were significantly changed following injury (one-way between-subject ANOVA, $p < 0.05$) (**Figure 7a; Table supplement 1**). Confirming that the transcription response *in vitro* recapitulated *in vivo* findings, we found Jun upregulated 1.41 fold in our microfluidic cultures 24 h post-axotomy [18].

Trans-synaptic mediators down-regulated post-axotomy

Next we sought to identify potential trans-synaptic mediators that may influence synaptic vesicle release at synapses onto injured neurons. We focused on differentially expressed transcripts that are known to localize to cell-cell contacts, such as synapses (**Figure 7b**). Within this category, only 6 transcripts were significantly changed. These transcripts included podoplanin (*Pdpn*), kinesin family member 26B (*Kif26b*), cadherin 24 - type2 (*Cdh24*), myosin X (*Myo10*), netrin-1 (*Ntn1*) and intercellular adhesion molecule2 (*Icam2*). We found that *Ntn1* was significantly downregulated in our microarray results, consistent with published findings that netrin family proteins are downregulated following SCI in adult rats [33]. Netrin-1 is a secreted axon guidance and synaptogenic cue that is enriched at mature dendritic spines [34] and is known to induce synaptic DCC clustering and enhance synapse maturation [35].

Exogenous netrin-1 normalizes injury-induced spine density and presynaptic release

The downregulation of netrin-1 following injury led us to ask whether adding exogenous netrin-1 might rescue, to some degree, the axotomy-induced synaptic changes. To test this we applied exogenous netrin-1 to the somatodendritic compartment 40 h after axotomy and evaluated the resulting changes in spine density, synaptic vesicle release and responsiveness at 48 h post-axotomy. We performed live imaging of somatodendritic domains before and after axotomy to measure spine density changes and found that netrin-1 treatment for 8 h was sufficient to normalize spine density to pre-axotomy levels (**Figure 8a,b**). We then used FM dyes to compare presynaptic release properties between axotomized and uninjured controls. Exogenous netrin-1 increased the total number of FM

puncta at 48 h post-injury to levels found in uninjured controls and reduced the percentage of responsive puncta to levels found in uninjured controls (**Figure 8c,d**). We next tested whether netrin-1 might rescue axotomy-induced disinhibition. Netrin-1 treatment following axotomy normalized the density of inhibitory terminals (vGAT labeled) at axotomized neuron without significantly altering the density of glutamatergic terminals (vGLUT1 labeled) (**Figure 8e,f**).

Because DCC levels parallel netrin-1 expression changes [36, 37], we next confirmed that DCC levels were downregulated at synapses formed onto the somatodendritic domain of axotomized neurons (**Figure 8g,h**). Local synaptic DCC immunofluorescence at spines of axotomized neurons were decreased at 48 h post-injury. Further, application of exogenous netrin-1 normalized synaptic DCC levels to that similar to uninjured controls (**Figure 8g,h**).

If downregulation of netrin-1 signaling regulates axotomy-induced synaptic remodeling, we would expect that blocking netrin-1 signaling in uninjured neurons would be sufficient to cause both reductions in spine density and the density of inhibitory terminals. Spine density in uninjured cultures treated with a DCC function blocking antibody for 24 h was significantly reduced after treatment while control chambers treated with an IgG control were not. Further, we found that blocking DCC was sufficient to cause a reduction in the density of vGAT puncta per eGFP-filled neuron area. Together, our data suggest that netrin-1 signaling may play a critical role in regulating synaptic remodeling following axonal damage, including in modulating inhibition following injury.

Discussion

We developed a model system to study the cellular mechanisms of synaptic remodeling following axon injury in cultured long projection pyramidal neurons. Importantly, this *in vitro* model system recapitulates hallmarks of neurons subjected to axonal injury *in vivo*, including chromatolysis [6, 20], retrograde spine loss [4, 21, 22], retrograde hyper-excitability [1-3], and disinhibition [2, 9, 10]. In addition, axotomy-induced transcriptional changes in this *in vitro* model are consistent with *in vivo* findings [7, 19]. This *in vitro* model system provides a unique tool to examine axotomy-induced retrograde signaling intrinsic to neurons and the resulting effects to interneuronal communication.

While axon regeneration following injury is extensively studied, much less is known about how proximal neurons within the mammalian brain are affected following axonal damage [38] and more specifically how synapses onto injured neurons are remodeled. Our results suggest that axotomy-induced retrograde synaptic remodeling requires local signaling mediated by sodium and/or calcium influx at the site of injury to activate a rapid transcriptional response. Both post-synaptic dendritic spine loss and trans-synaptic changes in presynaptic inputs required transcription in axotomized pyramidal neurons. Our data is consistent with axonal injury signaling in other model systems. Localized reversal of a sodium calcium exchanger (NCX) at the site of injury may amplify calcium influx and contribute to long range signaling. Supporting this, blocking sodium channels with TTX and the reversal of NCX, reduced axonal damage of mouse peripheral sensory neurons [39]. There is evidence that a calcium wave may locally can propagate to the nucleus to induce a transcriptional response in peripheral neurons [40].

Alternatively, the localized influx of calcium may also be a priming effect for retrograde transport of signaling complexes required to initiate transcription [6].

The sequential post- and then pre- synaptic changes following axotomy suggest a trans-synaptic mechanism. Axotomy-induced spine loss was followed by a preferential loss of inhibitory inputs and an increase in spontaneous release of both excitatory and inhibitory inputs. These post- and then pre- synaptic changes are consistent with the involvement of synaptic homeostasis where retrograde molecules are released post-synaptically to influence presynaptic release. Further support for the involvement of trans-synaptic mechanisms comes from our observation of an increase in spontanenous neurotransmitter release localized at excitatory synapses onto axotomized neurons, but not at neighboring excitatory synapses onto uninjured neurons. The significantly enhanced firing rate following SCI in cortical layer Vb, but not layers Va and VI, provides additional support for this specificity.

Dendritic release of secreted proteins (e.g., BDNF, NT-3 and NT-4) and diffusible molecules, such as nitric oxide, can trans-synaptically regulate neurotransmitter release [41-43]. Injury of motoneurons from myocytes caused synaptic remodeling of inputs to motoneurons involving nitric oxide synthesis [44]. While these previously reported trans-synaptic signaling pathways were not detectably altered in our microarray analysis, we did identify the secreted protein, netrin-1, as significantly downregulated in our axotomized cultures 24 h post- axotomy. Netrin-1 is secreted locally from target cells and signals DCC receptors that are present along axons [35] to influence presynaptic release and maturation [45, 46]. While netrin-1 signaling is historically thought of in a developmental context, there is increasing evidence of the importance of netrin-1 signaling in the adult

CNS. Consistent with our *in vitro* findings, netrin family members are downregulated *in vivo* following spinal cord injury in adult rats [33, 47] and DCC remains persistently low after 7 months post-injury in adult rats [33]. Netrin-1 has also recently been tested as a potential therapeutic agent following injury and has been shown to improve recovery outcomes [48-50].

Our data show that adding exogenous netrin-1 one and a half days after axotomy dramatically increased spine density and the density of inhibitory terminals to levels found in uninjured controls. The restoration of inhibitory terminals in axotomized samples treated with netrin-1 is a novel and exciting finding. Evidence from C.elegans confirms a link between netrin-1 signaling and stabilization of $GABA_A$ receptors [51]. Yet, it remains unclear how netrin-1 signaling modulates inhibitory input and will be an important topic for future studies. Interestingly, specific loss of inhibitory, and not excitatory, terminals suggests that orphaned excitatory inputs may remain available for some period of time to form new connections. Large headed dendritic spines could also receive multiple excitatory inputs, stabilizing them, and allowing them to find new partners over time.

Axonal damage within the CNS occurs in numerous disorders and diseases, but little is known about the overall impact on cortical circuit function. Importantly, our cell-based findings have broader applicability beyond spinal cord injury to numerous conditions where axonal damage is prevalent, such as other forms of traumatic brain injury, Alzheimer's disease, and multiple sclerosis. Further, remodeling is enhanced in embryonic or neonatal neurons, making the use of an *in vitro* approach using these

426 neurons, together with *in vivo* models, advantageous for identifying pathways
427 instrumental for neurological recovery [52].
428

429 **Materials and Methods**

430 *Hippocampal cultures.* Animal procedures were carried out in accordance with
431 the University of North Carolina at Chapel hill Institutional Animal Care and Use
432 Committee (IACUC). Dissociated hippocampal cultures were prepared from Sprague
433 Dawley rat embryos (E18-E19) as previously described [13, 23] with the following
434 modifications. Hippocampal tissue was dissected in dissociation media (DM) containing
435 82 mM Na_2SO_4, 30 mM K_2SO_4, 5.8 mM $MgCl_2$, 0.25 mM $CaCl_2$, 1 mM HEPES, 20 mM
436 Glucose and 0.001% Phenol red. For enzymatic digestion, equal volumes of TrypLE
437 Express (Invitrogen) and DM were added to the tissue and incubated at 37°C for 8 min.
438 Tissue was then rinsed and gently triturated in neuronal culture media consisting of
439 Neurobasal media (Invitrogen) supplemented with 1x B27 (Invitrogen), 1x Antibiotic-
440 antimycotic (Invitrogen), 1x Glutamax (Invitrogen). Dissociated cells were resuspended
441 in neuronal culture media to yield $12x10^6$ cells per ml.
442

443 *Microfluidic chambers.* Poly(dimethylsiloxane) (PDMS) microfluidic chambers
444 were replica molded from microfabricated master molds as described previously [13]. All
445 experiments used chambers with 900 μm long microgrooves to separate the
446 somatodendritic and axonal compartments as described previously [13, 14, 23]. Microfluidic
447 chambers were placed onto glass coverslips coated with 500-550 kDa Poly-D-Lysine
448 (BD Biosciences). Approximately ~90,000 cells were plated into the somatodendritic

449 compartment and axons extended into the adjacent axonal compartment after 5-7 days of
450 culture. Axotomy was performed between 11 and 15 days in vitro (DIV) according to
451 previously published procedures [13, 14]. Briefly, media was first removed from the axonal
452 compartment and stored for future use. The axonal compartment was then aspirated until
453 completely devoid of fluid. The stored culture media was then returned immediately to
454 the axonal compartment for the duration of the culture time. Microfluidic devices with
455 equivalent viable cell populations were randomly chosen for either axotomy or uninjured
456 control groups.
457
458 *Retrograde labeling.* Retrograde labeling was performed using either modified
459 cholera toxin or rabies virus. Cholera Toxin Subunit B Alexa Fluor 488 or 568 (Life
460 technologies, Molecular Probes; 1 µg in 200 µl of neuronal culture media) was added to
461 the axonal compartment of the microfluidic chamber and incubated for ~ 15 h at 37°C.
462 After 15 h of incubation, the axonal compartment media was removed, rinsed and
463 replaced using fresh neuronal culture media before performing axotomy or imaging.
464 G-deleted Rabies-mCherry or GFP virus [53] (Salk Institute; $1x10^5$ viral units) in 50
465 µl- conditioned media was added to the axonal compartment of each chamber and
466 incubated for 2h at 37°C. Conditioned media was added back to the axonal compartments
467 following two washes with fresh NBE media. Chambers were maintained in 37°C
468 incubator for ~48 h until fluorescence expression was visible.
469
470 *Cell viability assay.* Dead cells were labeled using SYTOX Green (Invitrogen) at
471 a final concentration of 1 µM and all cell nuclei were labeled with NucBlue Hoechst

472 Stain (Invitrogen). Cells were incubated with SYTOX/Hoechst solution simultaneously in
473 1x PBS for 5 min at 37°C, washed with PBS, and fixed with 4% paraformaldehyde (PFA)
474 in PBS containing 40 mg/ml sucrose, 1 μM $MgCl_2$ and 0.1 μM $CaCl_2$ for 15 min at room
475 temperature (RT). Coverslips were then rinsed three times with PBS and mounted onto
476 the glass slide using Fluoromount G (Southern Biotech). SYTOX positive ($Sytox^+$) cells
477 were manually counted in ImageJ using sum projected z-stack confocal images. Percent
478 cell viability is calculated using [($Sytox^+$ - Hoechst) / Hoechst] * 100.
479
480 *Nissl Staining.* Neuronal cultures retrogradely labeled with Cholera Toxin were
481 either axotomized or left uninjured. PDMS chambers were carefully lifted off from PDL
482 coated coverslips 24 h post-axotomy. Cultures on the coverslips were quickly rinsed
483 twice with PBS, fixed with 4% PFA for 30 min at RT, washed twice in PBS, and
484 incubated in 0.1% Triton X-100/PBS for 10 min at RT. Cultures were incubated for 20
485 min in NeuroTrace 500/525 Green Fluorescent Nissl Stain (1:100; Invitrogen) and
486 washed for 10 min in 0.1% Triton X-100/PBS. Cell nuclei were stained with DAPI
487 (Sigma-Aldrich), rinsed three times in PBS, and then the coverslip was mounted onto a
488 microscope slide using Fluoromount G.
489
490 *Immunocytochemistry.* PFA fixed neuronal cultures were permeabilized in 0.25%
491 Triton X-100 and blocked in 10% normal goat serum for 15 min each. Coverslips were
492 incubated with anti-MAP2 (1:1000; Millipore # AB5622), anti-beta tubulin III
493 (1:2000;Aves # TUJ), anti-GAD67 (1:2000; Aves labs # GAD), anti-vGLUT1 (1:100;
494 NeuroMab, clone N28/9, cat. # 75-066), anti-vGAT (1:1000; Synaptic Systems # 131

003), anti-DCC (1:100; Calbiochem # OP45), or anti-synapsin1 (1:500; Calbiochem # 574778) primary antibodies in 1% blocking solution for overnight at 4°C. Coverslips were then incubated with goat anti-rabbit or goat anti-mouse or anti-chicken secondary antibodies conjugated to Alexa-fluorophores (1:1000; Invitrogen) for 1h at RT. Following PBS washes coverslips were mounted onto the glass slide.

RNA isolation. Total RNA from each of 3 axotomized chambers and 3 sham manipulated chambers (6 total samples) was isolated from the somatodendritic compartment of 14 DIV cultures, 24 h after manipulation. RNA was collected from the entire somatodendritic compartment for our gene expression analysis; thus, a fraction of neurons in the axotomized chambers were axotomized and the remaining fraction uninjured or "uncut". RNA was isolated using an RNAqueous-Micro Kit (Ambion) according to the manufactures instructions including DNase treatment, with modifications specific to accessing the microfluidic compartment [14]. Briefly, 50 µl lysis solution was added to one somatodendritic well and collected from the other somatodendritic well after solution flowed through the somatodendritic compartment to this adjacent well. Lysate was added to 50 µl of fresh lysis solution and mixed well by careful pipetting. Further RNA purification steps were performed according to the manufacturer's guidelines. Samples were maintained at -80ºC until prepared for microarray gene expression.

Microarray analysis. Quantification of RNA integrity and concentration was confirmed with an Agilent TapeStation 2200 at the UNC Lineberger Comprehensive

Cancer Center Genomics Core. Microarrays were processed at the UNC School of Medicine Functional Genomics Core using the Affymetrix GeneChip WT Plus Reagent Kit for cRNA amplification, cDNA synthesis, fragmenting and labeling. Samples were hybridized to Rat Gene 2.0 ST Arrays (Affymetrix). Data analysis was performed with Affymetrix Expression Console software and Affymetrix Transcriptome Analysis Console v2.0 software to compare axotomized cultures to uninjured control samples using one-way between-subject ANOVA of normalized intensities. Because a fraction of the harvested cells were axotomized in our axotomized samples, we used modest fold change values for defining our list of significantly changed transcripts (fold change absolute value ≥ 1.1 and ANOVA p-value <0.05). To identify cell-cell adhesion transcripts we searched for the biological process gene ontology category 'cell-cell adhesion'. Fold change shown in **Figure 7** was calculated by dividing the mean $\log_2$ intensity value of the uninjured control by the mean $\log_2$ intensity value of the axotomized culture samples.

Image acquisition and dendritic spine analysis. High-resolution z-stack montages of mCherry or GFP labeled live neurons were captured using Zeiss LSM 780 (63x 1.4 NA or 40x 1.4 NA oil immersion objective). Fluorescently labeled fixed neurons (**Figure supplement 2)** were captured using Olympus IX81 microscope (60x 1.3 NA silicon oil immersion objective). Dendrite and spine measurements from montages of fixed (**Figure supplement 2**) or live neurons were analyzed as described below. In live imaging, we captured " 0 h or before axotomy" confocal z-stack images using a 40x and 63x objective to create montages of neurons extending axons into the axonal compartment. Blinding

during group allocation was not feasible because same neurons were followed before and after axotomy. Axotomy was performed on the same day after acquiring these images. Images were acquired from same neuron 24 h post-axotomy. In some cases, images were also acquired from same neurons at 48 h post-axotomy (**Figure 1, 2 and 8**). Calibrated z-stack montages were analyzed for all dendrite and spine parameters. Dendrites were traced using semiautomatic neurite tracing tool, Neuron J [54, 55]. Dendrites greater than 10 μm in length were used in the analysis and were quantified for total dendrite length and number of branch points. Branch point numbers were calculated as the difference between the total number of dendrites and the number of primary dendrites. The number of spines on all primary dendrites of each neuron were manually labeled and categorized as thin, stubby or mushroom shaped using Neuron studio [56]. Spine density was calculated for 10 μm length of dendrite as [(# of spines / dendrite length)*10].

FM dye experiments and analysis. Cultures in microfluidic chambers at 24 h (14 DIV), 48 h (15 DIV), and 4d (17 DIV) post-axotomy were loaded with lipophilic dye FM® 5-95 (Invitrogen) using KCl mediated depolarization as described previously [23]. Briefly, cultures were first incubated for 30 min with pre-warmed HEPES-buffered solution (HBS; 119 mM NaCl, 5 mM KCl, 2 mM $CaCl_2$, 2 mM $MgCl_2$, 30 mM glucose, 10 mM HEPES). Media was then replaced with FM dye loading solution containing 10 μM FM 5-95, 20 μM AMPAR antagonist 6-cyano-7-nitroquinoxaline-2,3-dione disodium (CNQX; Tocris), 50 μM NMDAR antagonist D-(-)-2-amino-5-phosphonopentanoic acid (D-AP5; Tocris) in 90 mM KCl HBS for 1 min. The loading solution was replaced with HBS containing 10 μM FM 5-95 for 1 min and later rinsed

three times with a high-Mg^{2+}, low-Ca^{2+} solution (106 mM NaCl, 5 mM KCl, 0.5 mM $CaCl_2$, 10 mM $MgCl_2$, 30 mM glucose, 10 mM HEPES) containing 1 mM Advasep-7 (Biotium) to remove extracellular membrane-bound FM. Finally, cultures were washed in HBS containing 20 µM CNQX and 50 µM D-AP5 for at least three times, 1 min each. Next, we stimulated the microfluidic chambers using extracellular electrodes by placing a positive and negative electrode in each well of the somatodendritic compartment.

Electrical stimulation was provided by an AD Instrument 2 Channel Stimulus Generator (STG4002) in current mode with an asymmetric waveform (-480 µA for 1 ms and +1600 µA for 0.3 ms) for ~ 1 min at 20 hz for 600 pulses. The FM 5-95 imaging was performed as described previously using a spinning disk confocal imaging system [23]. Z-stacks (31 slices) were captured every 15 s during the baseline (1 min), stimulation (1 min), and after stimulation (2 min) periods. This stimulation pattern was optimized for efficient FM unloading within these microfluidic chambers and the frequency is greater than typically used in open well dishes. At least 3 baseline images were acquired before electrical stimulation. Sum projected confocal z-stack were converted to 8-bit images and registered using TurboReg, an image J plugin. We background subtracted the image stack using the image 3 min after stimulation. Image stacks thresholded to a pixel value of 15. FM puncta between 0.4 to 10 μm^2 were analyzed. We measured the intensity of each punctum in the whole field or specifically on GFP labeled neuron (**Figure 3a-c**) throughout all time-series (registered stack obtained by TurboReg, imageJ plugin). To analyze the unloading kinetics of FM puncta on GFP labeled neuron, we first thresholded the GFP image and then created an outline enclosing all the GFP labeled regions including spines. The outlined ROI was superimposed on the FM labeled image and the

intensity of each punctum in the selected ROI (GFP outline) was measured throughout all time series. We normalized fluorescence intensity of each puncta to the frame before stimulation. Puncta with >5% unloading after 1 min were used in the analysis as unloaded puncta. Time constants were estimated by curve fitting unloading kinetics to a single exponential decay function [23]. Curve fitting was done in MATLAB and FM puncta with time constants longer than 3 min were excluded from the analysis and assumed to be non-releasing. Number of FM puncta that unload >5% after 60s were classified as responsive using image stacks that were not background subtracted; puncta that did not meet this criteria were classified as unresponsive.

In activity and transcription blocking experiments, the FM 5-95 unloading experiment was performed as mentioned above at 48 h post-axotomy. The intensity measurements of each punctum in the whole field and subsequent analysis of FM unloading kinetics was performed as mentioned above.

Drug treatments. Local activity blockade solution (ABS), which includes low-Ca^{2+}, high-Mg^{2+}, and TTX (0.5 mM $CaCl_2$, 10 mM $MgCl_2$, 1 µM TTX) was applied soley to the axonal compartment for 1 h during axotomy (15 min prior and 45 min after axotomy). 5,6-dichloro-1-β-D-ribofuranosyl-1H-benzimidazole (DRB; Sigma-Aldrich # D1916) was suspended in DMSO and applied to the somatodendritic compartment at a final concentration of 80 µM for 1 h during axotomy (beginning 15 min prior to axotomy). Tetrodotoxin citrate (TTX; Tocris Bioscience # 1078) was suspended in HBS and applied to the somatodendritic compartment at a final concentration of 1 µM for 1 h during axotomy (beginning 15 min prior to axotomy). Media stored from the axonal

610 compartment prior to treatment was added back to the axonal compartment after
611 treatment. Exogenous netrin-1 was applied to the somatodendritic compartment after 1 $^{1}/_{2}$
612 day of axotomy, when spine changes were observed, at a final concentration of 625
613 ng/ml. A similar netrin-1 concentration has been used for cortical neurons over a
614 treatment time of 1-2 days to examine netrin-specific responses [57]. Netrin-1 was applied
615 for 8-10 h to observe stable synaptic changes. For DCC function blocking experiments,
616 anti-DCC (mDCC; Calbiochem # OP45) and isotype control (mIgG; BD pharmingen
617 #554121) was applied to the somatodendritic compartment of uninjured chambers at a
618 final concentration of 1 μg/ml for 24 h.
619
620 *Microscopy*. FM and fixed imaging was performed using CSU-X1 (Yokogawa)
621 spinning disk confocal imaging unit configured for an Olympus IX81 microscope (Andor
622 Revolution XD). Live imaging of neurons for spine analysis was captured using a Zeiss
623 LSM 780 confocal microscope with a Plan-Apochromat 40x objective (NA 1.4) at the
624 UNC Neuroscience microscopy core facility. Ligth excitation for the spinning disk
625 confocal imaging system was provided by 405 nm, 488 nm, 561 nm, and/or 640 nm
626 lasers. The following bandpass emission filters (BrightLine, Semrock) were used: 447/60
627 nm (TRF447-060), 525/30 nm (TRF525-030), 607/36 nm (TR-F607-036), 685/40 nm
628 (TR-F685-040). For FM imaging, the spinning disk confocal imaging system was used
629 with excitation at 561 nm and the 685/40 nm emission filter. We used 2x2 binning to
630 reduce the laser intensity and acquisition time for each frame; each z-stack was obtained
631 in ~5 s. For the Zeiss LSM 780, signal was acquired from up to three channels for GFP
632 (493 nm - 558 nm), Alexa 568 (569 nm - 630 nm), and Alexa 647 (640 nm - 746 nm).

633

634 *Whole-Cell Electrophysiology.* For whole-cell recordings, neurons were visually
635 identified with infrared differential interference contrast optics. Cells were recorded in
636 voltage-clamp configuration with a patch clamp amplifier (Multiclamp 700A), and data
637 were acquired and analyzed using pCLAMP 10 software (Molecular Devices). Patch
638 pipettes were pulled from thick-walled borosilicate glass with open tip resistances of 2–7
639 MΩ. Series and input resistances were monitored throughout the experiments by
640 measuring the response to a −5-mV step at the beginning of each sweep. Series
641 resistance was calculated using the capacitive transient at the onset of the step and input
642 resistance was calculated from the steady-state current during the step. Recordings were
643 sampled at 10 kHz and bessel filtered at 2 kHz. No series resistance compensation was
644 applied.

645 Prior to recording, microfluidic chambers and PDMS molds were removed and
646 the glass coverslips containing cells were mounted onto a submersion chamber,
647 maintained at 32º C. Cultures were perfused at 2 mL/min with artificial cerebrospinal
648 fluid (ACSF) containing 124 mM NaCl, 3 mM KCl, 1.25 mM Na_2PO_4, 26 mM $NaHCO_3$,
649 1 mM $MgCl_2$, 2 mM $CaCl_2$ and 20 mM d-(+)-glucose, saturated with 95% O_2, 5% CO_2.
650 To determine if recorded neurons' axons entered the microfluidic chamber, 0.035 mM
651 Alexa-594 was included in all internal solutions to allow for post-hoc visualization of
652 neuronal morphology.

653 Events with a rapid rise time and exponential decay were identified as mEPSCs or
654 mIPSCs respectively using an automatic detection template in pCLAMP 10, based on
655 previously published methods[58]. mEPSC events were post-hoc filtered to only include

656 events with a peak amplitude ≥5 pA and a ≤3 ms 10-90% rise time. Mean mEPSC
657 parameters were quantified from a 10 min recording period and mIPSC parameters were
658 sampled from a 5 min recording period. Neurons were excluded from analysis if R_{series}
659 was >25 MΩ during anytime during the recording.
660
661 *mEPSCs Recordings.* mEPSC recordings were performed similar to previously
662 described[59]. AMPAR-mediated mEPSCs were isolated by voltage-clamping neurons at -
663 70 mV and by supplementing the ACSF with TTX citrate (1 μM, Abcam), the GABA (A)
664 receptor antagonist picrotoxin (50 μM, Sigma-aldrich), and the NMDA receptor
665 antagonist D, L-2-amino-5 phosphonopentanoic acid (100 μM, AP5, Abcam). The
666 internal solution contained: 100 mM $CsCH_3SO_3$, 15 mM CsCl, 2.5 mM $MgCl_2$, 5 mM
667 QX-314-Cl, 5 mM tetra-Cs-BAPTA, 10 mM HEPES, 4 mM Mg-ATP, 0.3 mM Na-GTP,
668 and 0.5% (w/v) neurobiotin with pH adjusted to 7.25 with 1 M CsOH and osmolarity
669 adjusted to ~295 mOsm with sucrose.
670
671 *mIPSC recordings.* mIPSCs were isolated by supplementing the ACSF with TTX
672 citrate (1 μM), the NMDA receptor antagonist AP5 (100 μM), and the AMPA/Kainate
673 receptor antagonist 6,7-dinitroquinoxaline-2,3-dione (20 μM, DNQX, dissolved in
674 DMSO for a final concentration of 1% v/v DMSO in ACSF, Abcam). For mIPSC
675 recordings, the pipette solution contained a relatively lower chloride concentration,
676 similar to intracellular chloride concentrations that are present in more mature neurons [60].
677 This pipette solution contained, 110 mM $CsCH_3SO_3$, 2.5 mM $MgCl_2$, 5 mM QX-314-Cl,
678 5 mM tetra-Cs-BAPTA, 10 mM HEPES, 4 mM Mg-ATP, 0.3 mM Na-GTP, and 0.5%

679 (w/v) neurobiotin with pH adjusted to 7.28 with 1 M CsOH and a 300 mOsm osmolarity.
680 Following break-in, neurons were first voltage-clamped at -70 mV for at least three
681 minutes to allow dialysis with pipette solution, after which the voltage was gradually
682 changed to 0 mV, where it was maintained for duration of the recording.
683
684 *SCI injury and in vivo electrophysiology.* Nineteen adult male, Fischer-344 inbred
685 rats (Harlan Laboratories, Indianapolis, IN) were selected for this study. A total of 14 rats
686 received a contusion injury in the thoracic cord at level T9–T10, whereas 5 rats were
687 randomly selected as uninjured controls. After a minimum of 4 weeks following SCI,
688 intracortical microstimulation (ICMS) and single-unit recording techniques were used in
689 the hindlimb motor area (HLA) to determine movements evoked by ICMS and spike
690 rates. The protocol was approved by the University of Kansas Medical Center
691 Institutional Animal Care and Use Committee.
692 Spinal cord surgeries were performed under ketamine hydrochloride (80
693 mg/kg)/xylazine (7 mg/kg) anesthesia and aseptic conditions. Each of the SCI rats
694 underwent a T9–T10 laminectomy and contusion injury using an Infinite Horizon spinal
695 cord impactor (Precision Systems and Instrumentation, LLC, Fairfax Station, VA) with a
696 200 Kdyn impact. At the conclusion of surgery, 0.25% bupivacaine hydrochloride was
697 applied locally to the incision site. Buprenex (0.01mg/kg, SC) was injected immediately
698 after surgery and 1 day later. On the first week after surgery, the rats received daily
699 injections of 30,000U penicillin in 5mL saline. Bladders were expressed twice daily until
700 the animals recovered urinary reflexes.

Post-SCI surgical and neurophysiological procedures were conducted under aseptic conditions 4 to 18 weeks post-SCI. At the time of these procedures, ages ranged from 4.5 to 7.5 months. After an initial, stable anesthetic state was reached using isoflurane anesthesia, isoflurane was withdrawn and the first dose of ketamine hydrochloride (100 mg/kg)/xylazine (5 mg/kg) was administered. The rats were placed in a Kopf small-animal stereotaxic instrument and a craniectomy was performed over the motor cortex. The dura was incised and the opening filled with warm, medical grade, sterile silicone oil. Core temperature was maintained within normal physiological limits using a feedback-controlled heating pad during the entire procedure. A stable anesthetic level was assessed by monitoring the respiratory and heart rate, and reflexes to noxious stimuli.

In each rat, neuronal recordings were begun at ~3 h after initiation of the procedure. Neuronal action potentials (single-units or spikes) were recorded with a single-shank, 16-channel Michigan-style linear microelectrode probe (Neuronexus, Ann Arbor, MI). A total of 15 channels were active in each procedure. The tip of the probe was lowered to a depth of 1720 μm below the cortical surface, allowing accurate determination of depth for each recording site. Because no hindlimb responses were evoked using ICMS in SCI rats, the location of HLA in SCI rats was determined by the stereotaxic coordinates derived in normal rats in a previous study (centered at 2mm posterior and 2.64mm lateral to bregma). At each cortical location, electrical activity was collected and digitized for 5 min from each of the 15 active sites using neurophysiological recording and analysis equipment (Tucker Davis Technologies, Alachua, FL). Neural spikes were discriminated using principle component analysis.

724 Sample waveforms (1.3 msec in duration) were collected that passed 5.5 X SD below
725 root mean square (RMS). After each experiment, the probe was cleaned with Opti-Free
726 solution (Alcon Laboratories, Fort Worth, TX), followed by ethanol and then rinsed
727 thoroughly in distilled water. The electrode impedance of each site remained at 0.9MΩ
728 for each experiment. At the end of the recording session, rats were humanely euthanized
729 with an overdose of sodium pentobarbital.
730
731 *Statistics.* Graphpad prism 6 statistical program was used. For calculating
732 significance on spine density in live imaging data, paired two-tailed t-test was performed.
733 Unpaired two-tailed t-test was performed when comparing two independent groups. For
734 FM unloading experiments and for comparing multiple groups, Two-way ANOVA and
735 One-way ANOVA were used respectively followed by Bonferroni post-hoc test. For
736 patch-clamp electrophysiology experiments, unpaired two-tailed t-tests or unpaired two-
737 tailed t-tests with Welch's correction were performed to compare two groups. For *in vivo*
738 experiments, hypotheses regarding spike firing rates were tested independently in each
739 cortical layer (Va, Vb and VI) using a two-tailed t-test, (alpha = 0.05). Samples were not
740 excluded from our data sets and sample size was determined based on our experience and
741 previous publications [23].
742
743 *Data availability.* The microarray data will be submitted to GEO and accession
744 numbers will be provided at the time of publication. All relevant data will be available
745 from authors upon request.
746

747 REFERENCES:

748 1. Nudo, R.J. *Front Hum Neurosci* 7, 887 (2013).

749 2. Takechi, U., *et al. Clin Neurophysiol* 125, 2055-2069 (2014).

750 3. Nudo, R.J. & Milliken, G.W. *J Neurophysiol* 75, 2144-2149 (1996).

751 4. Oudega, M. & Perez, M.A. *J Physiol* 590, 3647-3663 (2012).

752 5. Frost, S.B., *et al. J Neurophysiol* 89, 3205-3214 (2003).

753 6. Rishal, I. & Fainzilber, M. *Nat Rev Neurosci* 15, 32-42 (2014).

754 7. Urban, E.T., 3rd, *et al. Molecular and cellular biochemistry* 369, 267-286 (2012).

755 8. Kim, B.G., *et al. Exp Neurol* 198, 401-415 (2006).

756 9. Jacobs, K.M. & Donoghue, J.P. *Science* 251, 944-947 (1991).

757 10. Ding, M.C., *et al. J Neurosci* 31, 14085-14094 (2011).

758 11. Nakatomi, H., *et al. Cell* 110, 429-441 (2002).

759 12. Will, B., *et al. Progress in Neurobiology* 72, 167-182 (2004).

760 13. Taylor, A.M., *et al. Nat Methods* 2, 599-605 (2005).

761 14. Taylor, A.M., *et al. J Neurosci* 29, 4697-4707 (2009).

762 15. Taylor, A.M., *et al. Neuron* 66, 57-68 (2010).

763 16. Banker, G.A. & Cowan, W.M. *Brain Res* 126, 397-342 (1977).

764 17. Benson, D.L., *et al. J Neurocytol* 23, 279-295 (1994).

765 18. Greer, J.E., *et al. J Neurosci* 32, 6682-6687 (2012).

766 19. Ikeda, S. & Nakagawa, S. *Brain Res* 792, 164-167 (1998).

767 20. McIlwain, D.L. & Hoke, V.B. *BMC Neurosci* 6, 19 (2005).

768 21. Ghosh, A., *et al. Cereb Cortex* 22, 1309-1317 (2012).

769 22. Gao, X., *et al. PLoS One* 6, e24566 (2011).

770 23. Taylor, A.M., *et al. J Neurosci* 33, 5584-5589 (2013).

771 24. Zakharenko, S.S., *et al. Nat Neurosci* 4, 711-717 (2001).

772 25. Frost, S.B., *et al. J Neurotrauma* 32, 1666-1673 (2015).

773 26. Lewicki, M.S. *Network* 9, R53-78 (1998).

774 27. Nudo, R.J., *et al. The Journal of Comparative Neurology* 358, 181-205 (1995).

775 28. Barron, K.D., *et al. J Neuropathol Exp Neurol* 47, 62-74 (1988).

776 29. Chen, J.L., *et al. Neuron* 74, 361-373 (2012).

777 30. Markram, H., *et al. Nat Rev Neurosci* 5, 793-807 (2004).

778 31. Chiu, C.Q., *et al. Science* 340, 759-762 (2013).

779 32. Higley, M.J. *Nat Rev Neurosci* 15, 567-572 (2014).

780 33. Manitt, C., *et al. J Neurosci Res* 84, 1808-1820 (2006).

781 34. Horn, K.E., *et al. Cell Rep* 3, 173-185 (2013).

782 35. Goldman, J.S., *et al. J Neurosci* 33, 17278-17289 (2013).

783 36. Xu, K., *et al. Science* 344, 1275-1279 (2014).

784 37. Manitt, C., *et al. J Neurosci* 29, 11065-11077 (2009).

785 38. Canty, A.J., *et al. J Neurosci* 33, 10374-10383 (2013).

786 39. Persson, A.K., *et al. J Neurosci* 33, 19250-19261 (2013).

787 40. Cho, Y., *et al. Cell* 155, 894-908 (2013).

788 41. Wong, Y.C. & Holzbaur, E.L. *J Neurosci* 34, 1293-1305 (2014).

789 42. Branco, T., *et al. Neuron* 59, 475-485 (2008).

790 43. Gonzalez-Forero, D. & Moreno-Lopez, B. *Neuroscience* 283, 138-165 (2014).

791 44. Sunico, C.R., *et al. J Neurosci* 25, 1448-1458 (2005).

792 45. Stavoe, A.K. & Colon-Ramos, D.A. *The Journal of Cell Biology* 197, 75-88
793 (2012).

794 46. Colon-Ramos, D.A., *et al. Science* 318, 103-106 (2007).

795 47. Ahn, K.J., *et al. Neurosci Lett* 419, 43-48 (2007).

796 48. Lu, H., *et al. Front Med* 5, 86-93 (2011).

797 49. Han, X., *et al. Mol Neurobiol* (2016).

798 50. Sun, H., *et al. Neurobiol Dis* 44, 73-83 (2011).

799 51. Tu, H., *et al. Neuron* 86, 1407-1419 (2015).

800 52. McKinley, P.A. & Smith, J.L. *J Neurosci* 10, 1429-1443 (1990).

801 53. Wickersham, I.R., *et al. Neuron* 53, 639-647 (2007).

802 54. Fu, M.M. & Holzbaur, E.L. *Autophagy* 10, 2079-2081 (2014).

803 55. Nagendran, T. & Hardy, L.R. *Neuroscience* 199, 548-562 (2011).

804 56. Rodriguez, A., *et al. PLoS One* 3, e1997 (2008).

805 57. Menon, S., *et al. Dev Cell* 35, 698-712 (2015).

806 58. Clements, J.D. & Bekkers, J.M. *Biophys J* 73, 220-229 (1997).

807 59. Larsen, R.S., *et al. Neuron* 83, 879-893 (2014).

808 60. Yamada, J., *et al. J Physiol* 557, 829-841 (2004).

809

810 **Acknowledgements:** We thank Stephanie Gupton for netrin-1, Kelly Carstens for
811 preliminary gene expression work, and Cassie Meeker for technical support. We thank
812 Richard Segal (MUSC), Julius Dewald (RIC) and Taylor lab members for their advice
813 and discussions. **Funding:** A.M.T. acknowledges support from the Eunice Kennedy
814 Shriver NICHD (K12 HD073945), NIMH (R42 MH097377), and an Alfred P. Sloan
815 Research Fellowship. Imaging was supported by the Confocal and Multiphoton Imaging
816 Core Facility of NINDS Center Grant P30 NS045892 and NICHD Center Grant (U54

817 HD079124). R.S.L was supported by NRSA predoctoral fellowship F31 MH091817 and
818 the UNC Department of Cell Biology and Physiology's Dr. Susan Fellner fellowship.
819 R.L.B. was supported in part by a grant from the National Institute of General Medical
820 Sciences under award 5T32 GM007092. **Author contributions:** T.N. designed and
821 performed experiments and wrote the manuscript. R.S.L. designed and performed
822 electrophysiology experiments. R.L.B. designed and performed experiments.. S.B.F.
823 performed experiments. B.D.P. designed experiments. R.J.N. designed and performed
824 experiments. A.M.T. designed experiments and wrote the manuscript. **Competing**
825 **financial interests:** Yes there is potential competing interest. A.M.T. is an inventor of
826 the microfluidic chambers (US 7419822 B2) and has financial interest in Xona
827 Microfluidics, LLC. T.N., R.L.B., R.S.L., R.J.N. and B.D.P. declare no competing
828 financial interests.
829

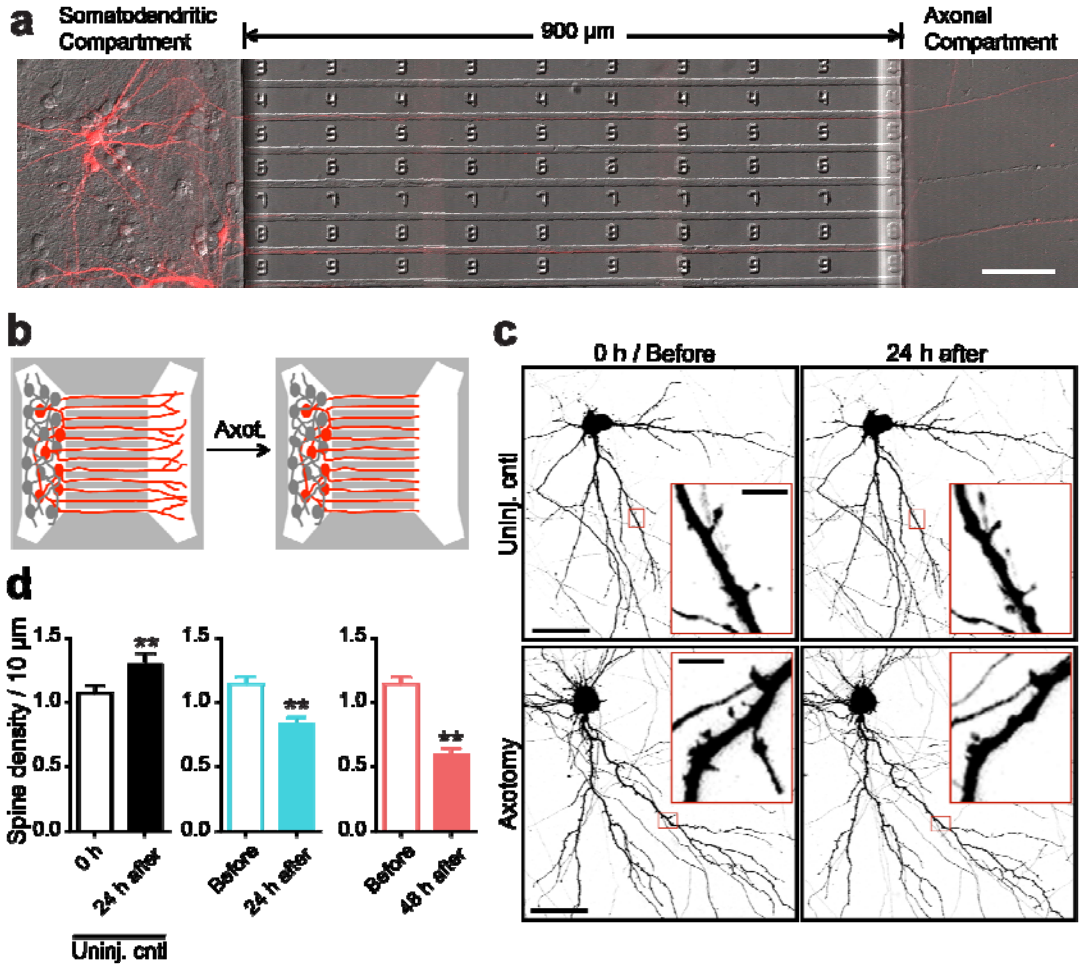

Figure 1: Distal axotomy of pyramidal neurons within microfluidic chambers induced dendritic spine loss on axotomized neurons. (**a**) 14 DIV rat hippocampal neurons cultured within a microfluidic chamber. Pyramidal neurons were retrogradely labeled using a G-deleted rabies mCherry virus added exclusively to the axonal compartment. (**b**) Cartoon illustration of *in vitro* axotomy (Axot.) within microfluidic chambers to selectively axotomize a subset of neurons (red) that extend axons through the microgroove region. Axons of uninjured neurons (grey) extend axons within the somatodendritic compartment. (**c**) Representative images of neurons and dendritic segments retrogradely labeled with G-deleted rabies-mCherry virus (inverted fluorescence) from repeated live imaging of uninjured control (Uninj. cntl) and

841 axotomized neurons. Axotomized neurons were imaged before axotomy on DIV 13
842 (before) and uninjured controls were also imaged on DIV 13 (0 h) and then both
843 conditions were imaged at 14 DIV (24 h after). Image and inset scale bars, 50 and 5 μm,
844 respectively. (**d**) Quantification of spine density before and after axotomy and in
845 uninjured controls as described in *(c)*. Paired two-tailed t-test, **$p \leq 0.001$; 20 primary
846 dendritic process were analyzed from 5 individual neurons over two-independent
847 experiments. Error bars, SEM.
848

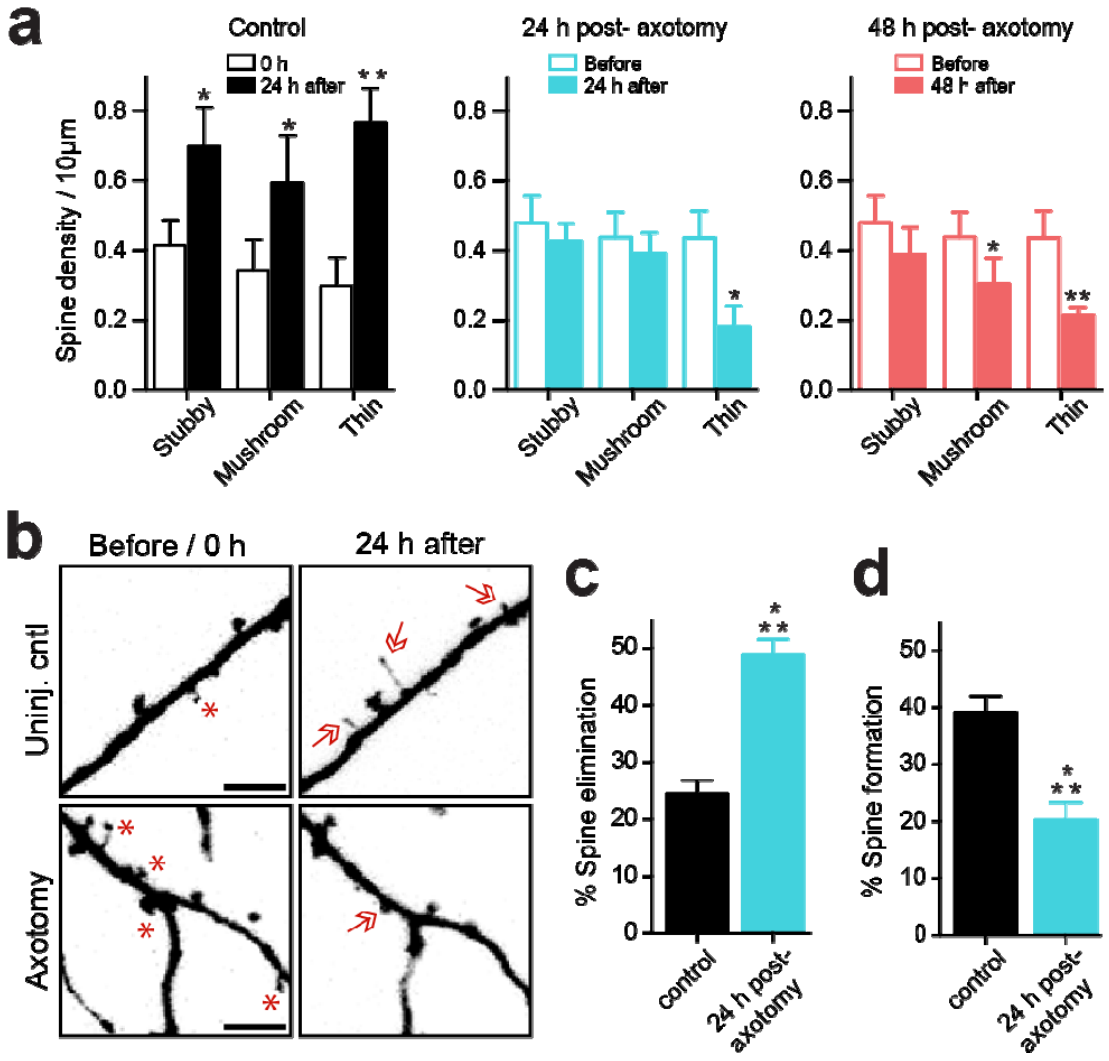

Figure 2: Axotomy led to dendritic spine loss and reduced new spine formation. (**a**) Quantification of spine density of stubby, mushroom, and thin spine categories before axotomy, 24 h post-axotomy, and 48 h post-axotomy and uninjured controls. Uninjured controls and axotomized samples were imaged beginning at 13 DIV (labeled "0 h" or "Before", respectively). Two-way ANOVA, Bonferroni post hoc test, * $p < 0.05$, ** $p < 0.01$. (**b**) Representative images of dendritic segments from uninjured control and axotomized neurons at 0 h or before axotomy, respectively, and 24 h after. Astericks indicate spines eliminated and arrows indicate formation of new spines. Scale bars, 5 µm.

858 (**c-d**) Bar graphs represent percentage of spines eliminated (c) and newly formed (d) after
859 24 h in uninjured controls (Uninj. cntl) and 24 h post-axotomy. Two-tailed t-test, *** p
860 <0.001. *(a,c,* and *d)* These analyses represent 20 primary dendritic processes from 5 live
861 neurons per condition over two independent experiments. The same trend was observed
862 in each independent experiment. Error bars, SEM.
863

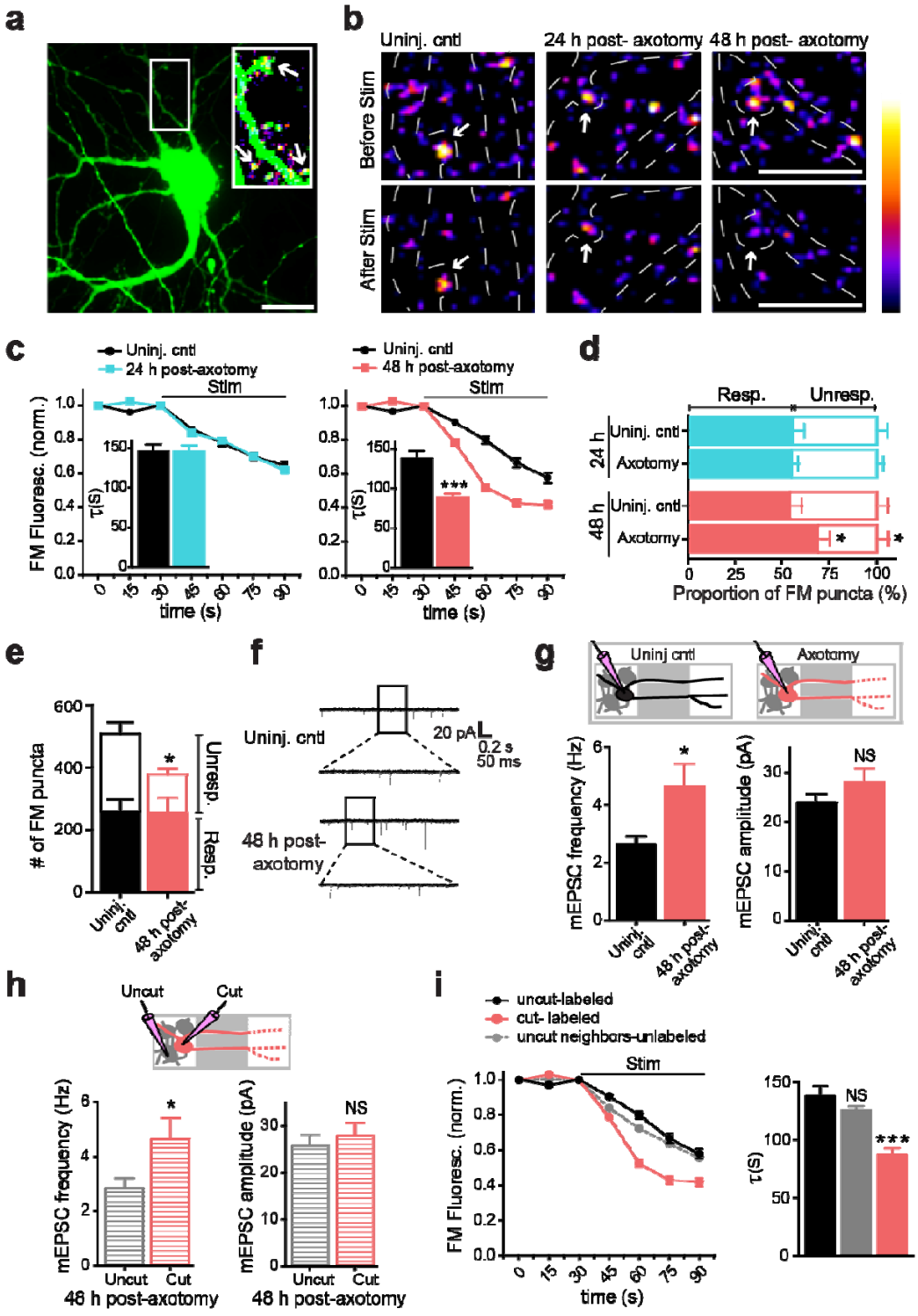

Figure 3: Distal axotomy induced a delayed trans-synaptic increase in presynaptic-excitability onto axotomized neurons. (**a**) Representative image of a neuron within the somatodendritic compartment of a microfluidic chamber retrogradely labeled with a

868 modified eGFP rabies virus applied briefly to the axonal compartment. Synaptic vesicle
869 release kinetics at axotomized neurons were quantified using FM dyes and analyzing the
870 subset of FM puncta that colocalize with the eGFP-filled neurons within the
871 somatodendritic region. Inset shows an enlarged region demonstrating colocalization of
872 FM puncta with eGFP-labeled dendrites and dendritic spines (arrows). FM puncta were
873 pseudocolored using the ImageJ 'fire' color look up table shown in *(b)*. Scale bar, 20 µm.
874 (b) Representative images show FM puncta before and after field stimulation. Boundaries
875 of eGFP labeled dendrites and spines are outlined as white dashed lines. Arrows in the
876 before and after stimulation images indicate destaining of FM labeled puncta at dendritic
877 spines. Scale bars, 10 µm. (**c**) FM unloading curves from FM puncta colocalized onto
878 GFP labeled neurons at 24 h post-axotomy (control, n=124 puncta combined from 3
879 chambers; axotomy, n=156 puncta combined from 3 chambers over 2 independent
880 experiments) and 48 h post-axotomy (control, n=160 puncta combined from 3 chambers;
881 axotomy, n=220 puncta combined from 3 chambers over 2 independent experiments).
882 Two-way ANOVA, Bonferroni post hoc test, ***$p \leq 0.001$. Insert: decay time constant
883 (τ) of FM puncta at 24 h and 48 h post-axotomy. Unpaired two-tailed t-test, ***$p < 0.001$.
884 (**d**) Percent responsive FM puncta and unresponsive FM puncta at 24 h (control, n=1,431;
885 axotomy, n=1,602; data shown are from 2 independent experiments which includes a
886 total of 4 chambers for each condition) and 48 h post-axotomy (control, n=3,452;
887 axotomy, n=2,793; data shown is from 3 independent experiments to yield a combined 7
888 chambers for each condition). Asterisks indicate that the percentage of responsive and
889 unresponsive puncta at 48 h post-axotomy is significantly different from control.
890 Unpaired two-tailed t-test, *$p < 0.05$. (**e**) Total number of responsive and unresponsive

FM puncta at 48 h post-axotomy (Resp: control, n=1,536; axotomy, n=1,522; Unresp: control, n=1,504; axotomy, n=742; data shown represents 3 independent experiments which combined included 6 chambers for each condition) Unpaired two-tailed t-test, *p< 0.05. (**f**) Representative traces of mEPSC recordings 48 h post-axotomy. (**g**) Quantification of mEPSC frequency and amplitude at 48 h post-axotomy (control, n=17 neurons; axotomy, n=20 neurons). Data shown were combined from 4 independent experiments. Unpaired two-tailed t-test with Welch's correction, *p < 0.05; mEPSC amplitude: unpaired two-tailed t-test, p = 0.2. Insert: Cartoon depicts recordings from either control neurons within uninjured chambers (*g*; black) or directly injured neurons within chambers subjected to axotomy (red). (**h**) Analysis of mEPSC frequency and amplitude from axotomy devices previously shown in (g) comparing neurons with axons that extended into the axonal compartment and were cut (cut, n=10 neurons), to neurons that did not extend axons into the compartment and were not cut (uncut, n=10 neurons). Unpaired two-tailed t-test with Welch's correction, *p < 0.05; mEPSC amplitude: unpaired two-tailed t-test, p = 0.52. Insert: Cartoon depicts recordings from either a directly injured neuron (*h*; red) or its neighboring uninjured neuron (grey). (**i**) FM unloading curves of neighboring uninjured neurons (uncut neighbors, n=767 puncta combined from 4 chambers) within axotomized chambers, identified by lack of eGFP labeling, were compared with uninjured control neurons (uncut) and axotomized neurons labeled with eGFP rabies virus. Two-way ANOVA, Bonferroni post hoc test ***p <0.001. Decay time constant (τ) of FM puncta at 48 h post-axotomy. One-way ANOVA, Bonferroni post hoc test ***p <0.001. Data shown represent 2 independent experiments. Error bars, SEM.

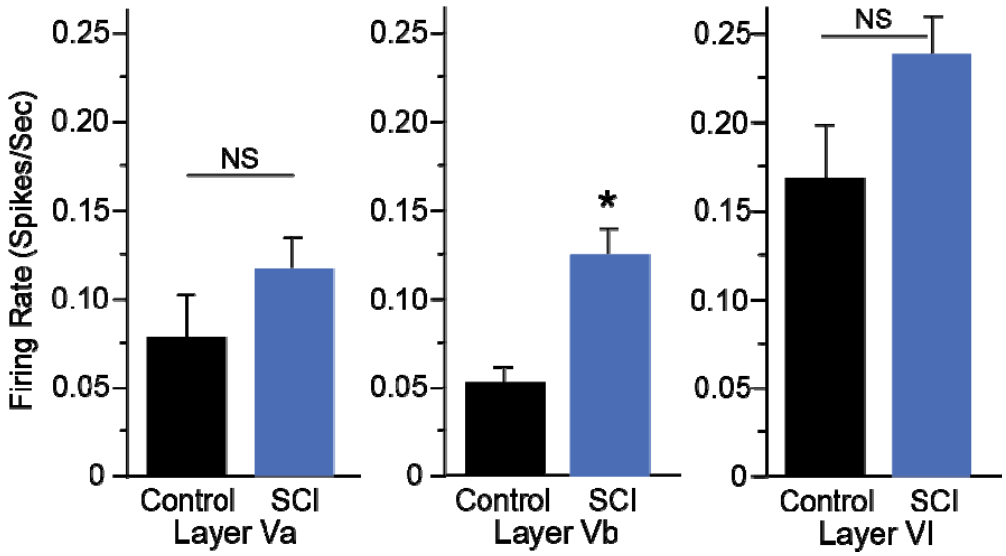

914 **Figure 4: Spinal cord injury results in increased spontaneous single-unit firing rate**

915 **in layer Vb of hindlimb cortex 4-18 weeks following injury.**

916 Mean spontaneous firing rates of isolated single-units in layers Va, Vb and VI of the

917 hindlimb motor cortex in control rats (n = 5) and rats with a spinal cord contusion at T9-

918 10 (n = 14). Laminar estimates are based on the depths of electrode sites on a single-

919 shank multi-electrode array relative to the cortical surface [25]. In each rat, single-unit

920 (spike) activity was sampled from 4 to 6 locations within the neurophysiologically-

921 identified hindlimb motor cortex. Data represent the mean firing rates of 1,744 isolated

922 units in Layers Va (control, n=124; SCI, n=312), Vb (control, n=155; SCI, n=390), and

923 VI (control, n=217; SCI, n=546). Asterisk indicates that the firing rate of single-units in

924 layer Vb of spinal cord injured rats is significantly higher compared to firing rates in

925 control rats. Two-tailed t-test, t=3.99, *p<0.0001.

926

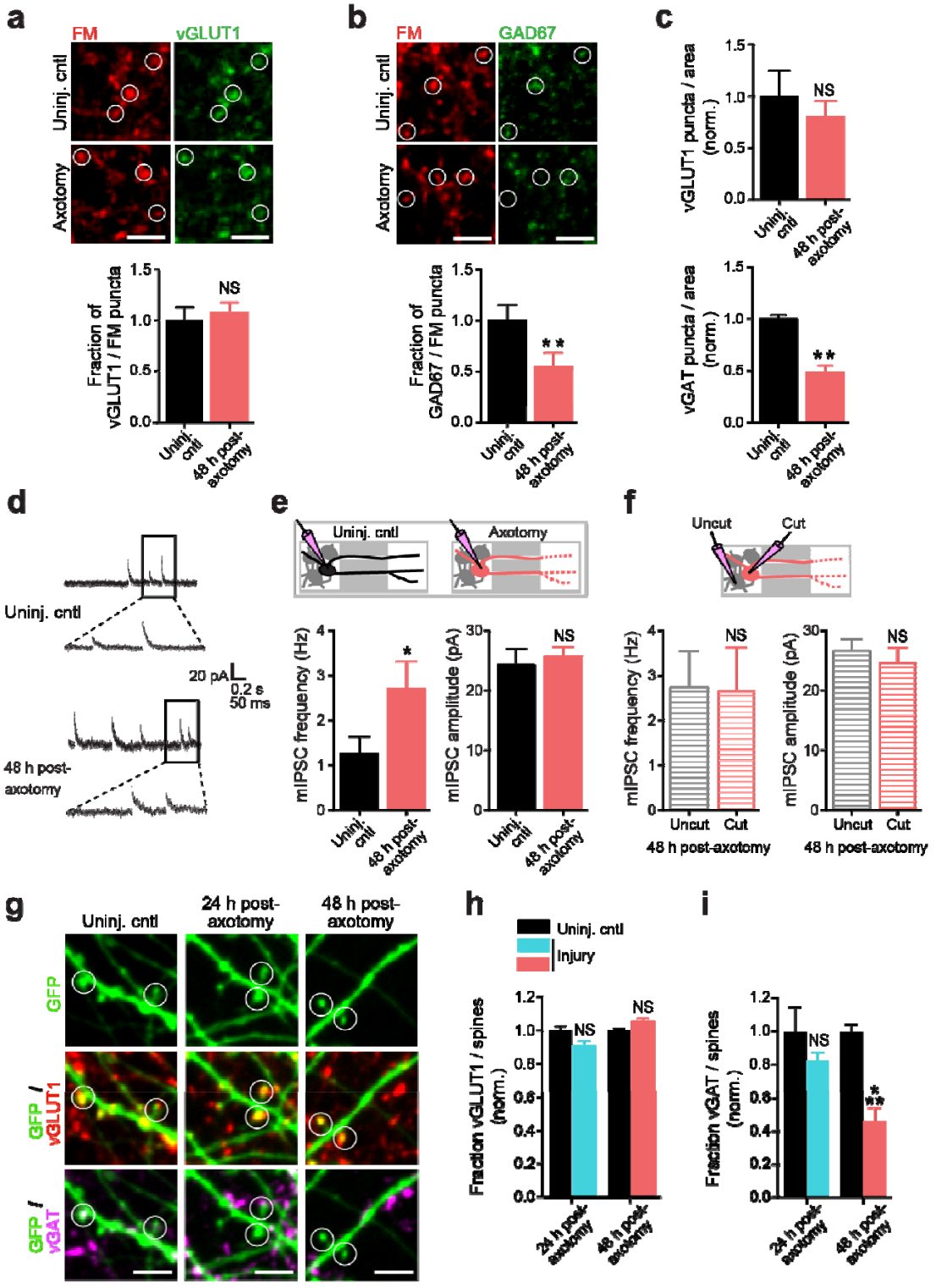

Figure 5: Distal axotomy induces culture-wide loss of inhibitory terminals, increased spontaneous GABAergic neurotransmission, and selective loss of inhibited spine synapses onto injured neurons. (**a**) Representative images showing fixable FM4-64FX

puncta (red) and vGLUT1 (green) labeling. White open circles highlight vGLUT1 expression in FM labeled terminals. Scale bars, 10 µm. vGLUT1 positive FM puncta at 48 h post-axotomy normalized to control. 10 individual fields from two chambers were analyzed per condition. (**b**) Images showing fixable FM4-64FX puncta (red) and GAD67 (green) labeling. White open circles highlight GAD67 expression levels in FM labeled terminals. Scale bars, 10 µm. Fraction of GAD67-positive FM puncta at 48 h post-axotomy normalized to control. 10 individual fields from two chambers were analyzed per condition. (**c**) Density of vGLUT1 and vGAT puncta in an area following 48 h post-axotomy, normalized to controls. N= 4 individual neurons were analyzed per condition. (*a-c*) Unpaired two-tailed t-test, **p < 0.01. (**d**) Representative traces of mIPSC recordings 48 h post-axotomy. (**e**) Quantification of mIPSC frequency and amplitude at 48 h post-axotomy (control, n=9 neurons; axotomy, n=17 neurons). Neurons from axotomized microfluidic devices have an increased mIPSC frequency compared to uninjured control devices (mIPSC frequency: unpaired two-tailed t-test with Welch's correction, p = 0.05; mIPSC amplitude: unpaired two-tailed t-test, p = 0.62). (**f**) Analysis of mIPSC frequency and amplitude from axotomy devices previously shown in (*e*) comparing neurons with axons that extended into the axonal compartment and were cut (cut, n=8 neurons), to neurons that did not extend axons into the compartment and were not cut (uncut, n=9 neurons). Axotomized neurons and their their uninjured neighbors from the same device have a similar mean mIPSC frequency and amplitude, suggesting axotomy increases spontaneous GABAergic neurotransmission both at injured and uninjured neighboring neurons (mIPSC frequency: unpaired two-tailed t-test, p = 0.94; mIPSC amplitude: unpaired two-tailed t-test, p = 0.51). (*d-f*) Data shown were combined

954 from 3 chambers. (**g**) Representative dendritic segments (retrogradely labeled with GFP)
955 showing spines that are labeled with either vGLUT1 (red) or vGAT (purple) antibodies.
956 White open circles highlight dendritic spines with vGLUT1 and/or vGAT synapses. (**h**)
957 Fraction of vGLUT1 positive dendritic spines at 24 h and 48 h post-axotomy normalized
958 to respective controls. (**i**) Fraction of vGAT positive dendritic spines at 24 h and 48 h
959 post-axotomy normalized to respective controls. 8 individual fields were analyzed per
960 condition from two independent experiments. The same trend was observed in each
961 experiment. Scale bars, 5 μm. Two-tailed t-test, ***$p \leq 0.001$. Error bars, SEM.
962

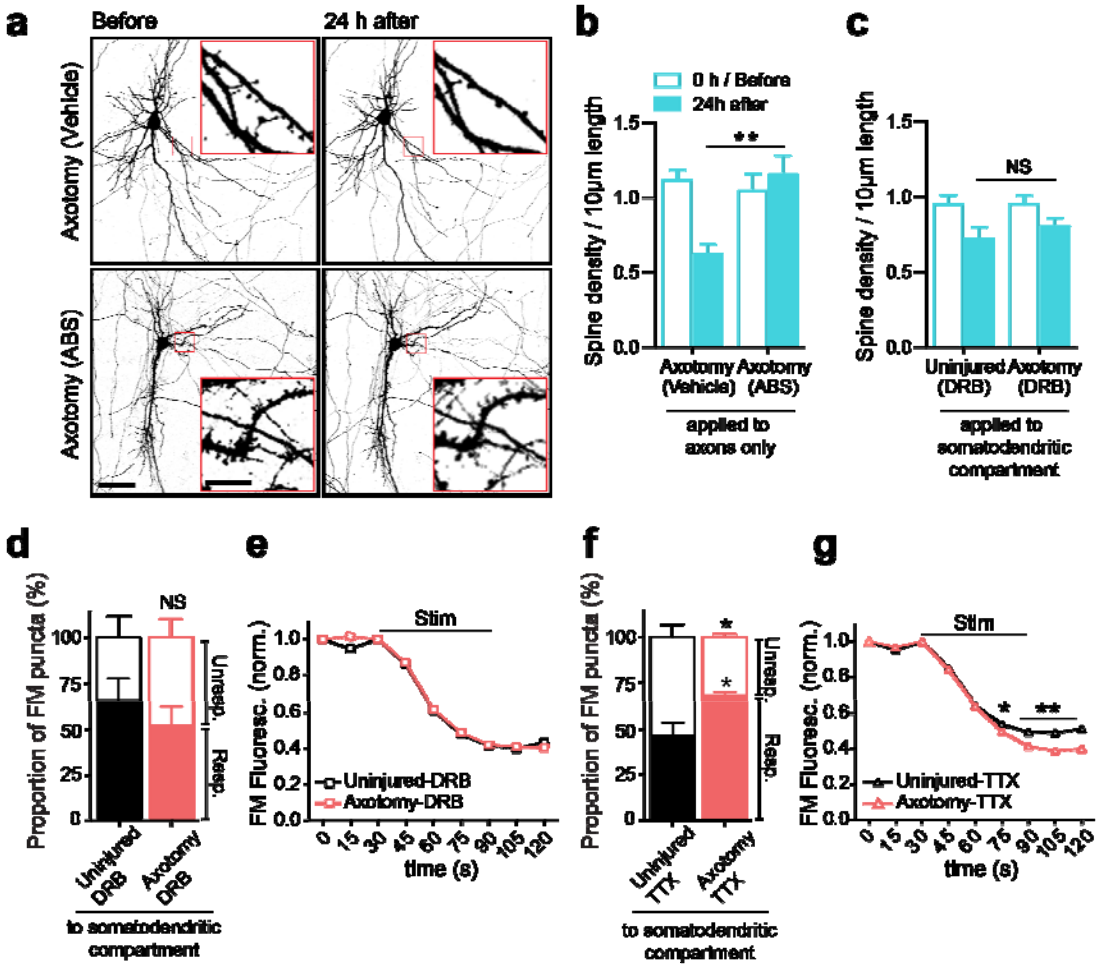

Figure 6: Injury-induced synaptic remodeling is triggered by retrograde propogation of injury signal from axon-to-soma and gene transcription.

(**a**) Representative images of neurons retrograde labeled with modified eGFP rabies virus (inverted grayscale) before and 24 h after axotomy in the presence of vehicle or local activity blockade solution (ABS) applied to axonal compartment for 1 h during axotomy. Axotomy and imaging were performed within microfluidic chambers. Inset shows zoomed in dendritic regions. (**b**) Quantification of spine density results described in (*a*). (**c**) Quantification of spine density changes following application of transcription blocker (DRB) to the somatodendritic compartment for 1 h during axotomy within microfluidic chambers. For (*b*,*c*) 20 primary dendritic process from 4 live neurons per condition were

974 analyzed over two independent experiments. Repeated measure two-way ANOVA,
975 Bonferroni post hoc test, **p<0.001. (**d**) Percent of unloaded FM puncta (responsive) and
976 unresponsive puncta at 48 h post-axotomy. Approximately 300 puncta were analyzed per
977 chamber; 4 individual chambers were analyzed per condition over two independent
978 experiments. Unpaired two-tailed t-test. (**e**) FM5-95 unloading following application of
979 DRB. Approximately 200 puncta were analyzed per chamber; 4 individual chambers
980 were analyzed per condition over two independent experiments. (**f**) Percent of unloaded
981 FM puncta (responsive) and unresponsive puncta at 48 h post-axotomy following
982 application of action potential blocker (TTX) to the somatodendritic compartment for 1 h
983 during injury. Approximately 400 puncta were analyzed per chamber; 4 individual
984 chambers were analyzed for each condition over two independent experiments. Asterisks
985 indicate that the percentage of responsive and unresponsive puncta is significantly
986 different compared to control. Unpaired two-tailed t-test, *p < 0.05. (**g**) FM5-95
987 unloading curves following application of TTX. Approximately 200 puncta were
988 analyzed per chamber; 4 individual chambers were analyzed for each condition over two
989 independent experiments). The same trend was observed in each pair of experiments.
990 Two-way ANOVA, Bonferroni post hoc test, *p < 0.05, **p < 0.01. Error bars, SEM.
991

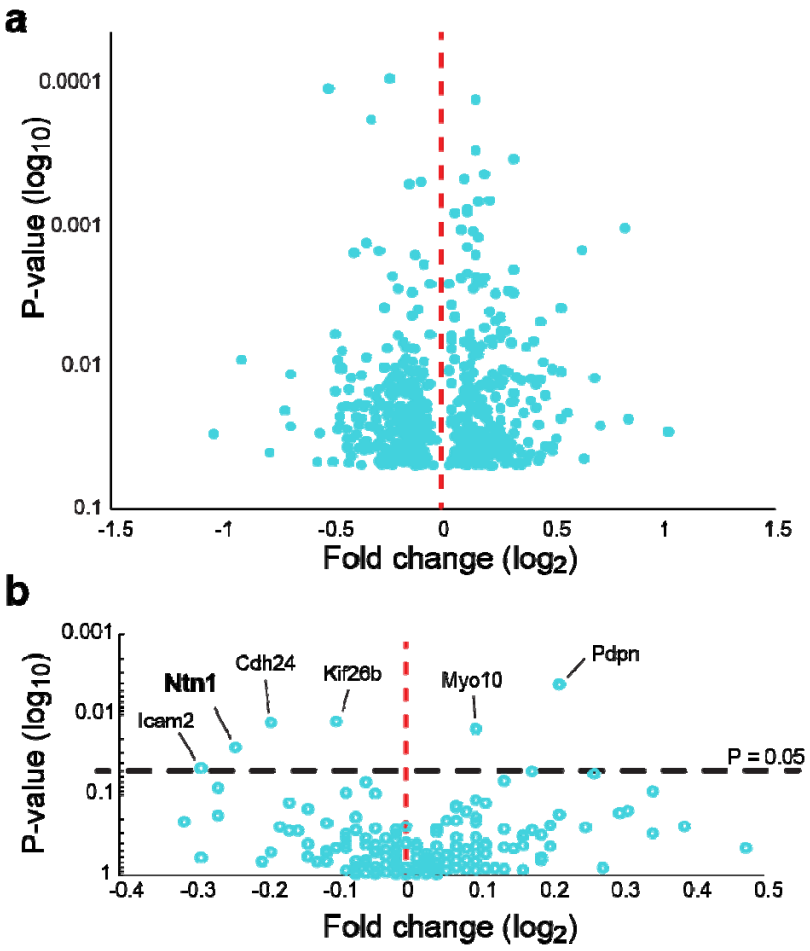

Figure 7: Cell-cell adhesion transcripts were differentially expressed within the somatodendritic compartment 24 h post-axotomy. Microarray analysis was performed on somatodendritic samples of controls and 24 h post-axotomy cultures. (**a**) Volcano plot showing differentially expressed RNAs that are significantly changed at 24 h post-axotomy (p-value < 0.05; n = 3 individual chambers each condition; **Table supplement 2**). (**b**) Volcano plot showing differential expression of transcripts from Gene Ontology biological process category "cell-cell adhesion". Only 6 transcripts are significantly changed in this category (**Table supplement 3**). One-way ANOVA, p-value < 0.05 represents the transcripts that are consistently changed in each of the three microarray datasets.

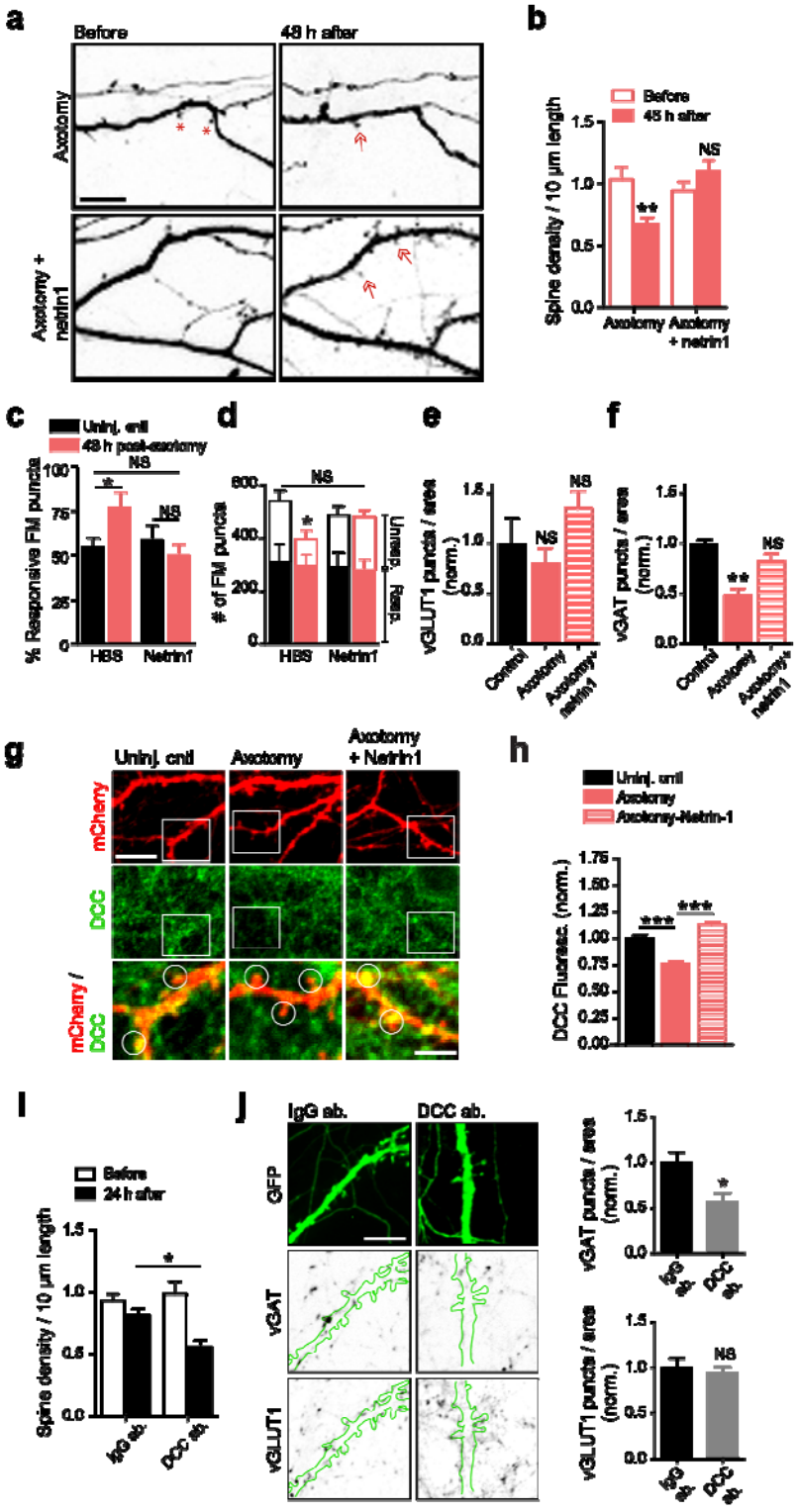

Figure 8: Exogenous netrin-1 rescues post and presynaptic changes following distal axotomy. (**a**) Representative images of dendritic segments within the somatodendritic

compartment before and 48 h after axotomy treated with either vehicle (HBS) or netrin-1 beginning at 40 h post-axotomy. Arrows indicate formation of new spines. Scale bars, 10 µm. (**b**) Quantification of spine density before and 48 h after axotomy and in response to exogenous application of netrin-1. Repeated measure two-way ANOVA, Bonferroni post hoc test, ** $p < 0.01$. Analysis included 20 primary dendrites from 5 live neurons per condition over two independent experiments. (**c**) The percent of responsive FM puncta (unloaded puncta) 48 h post-axotomy in cultures treated with vehicle (HBS) or netrin-1. Two-tailed t-test, *$p < 0.05$. (**d**) Average number of responsive and unresponsive FM puncta per field 48 h post-axotomy in cultures treated with vehicle (HBS) or netrin-1. (*c-d*) Approximately 400 puncta were analyzed per chamber from 7 individual chambers for each condition. Data shown was from two independent experiment and a similar trend was observed in each independent experiment. One-way ANOVA, Bonferroni post hoc test, *$p < 0.05$. Noticeably, injury increased the fraction of responsive FM puncta and exogenous application of netrin-1 normalized the fraction to levels found in untreated uninjured controls. (**e**) Density vGLUT1 and (**f**) vGAT puncta colocalizing within the fluorescently labeled somatodendritic regions retrograde labeled with rabies mCherry virus following vehicle (HBS) and exogenous netrin-1 application, normalized to vehicle controls. N= 4 individual neurons were analyzed per condition. One-way ANOVA, Bonferroni post hoc test,**$p < 0.01$. (**g**) Representative images of fixed dendritic segments, retrograde labeled with rabies mCherry virus and immunostained with DCC antibody following exogenous netrin-1 treatment. Regions of interest (ROI's; white circles) show synaptic DCC levels at 48 h post-axotomy. Scale bar, 10 µm. (**h**) Quantification of DCC fluorescence intensity at 48 h post-axotomy and in response to

exogenous application of netrin-1 (control, n=185 ROIs; axotomy, n=165 ROIs; axotomy + netrin-1, n=100 ROIs). At least 4 individual chambers were analyzed per condition from two independent experiments. The same trend was observed in each independent experiment. Two-way ANOVA, Bonferroni post hoc test, ***p < 0.001. (**i**) Quantification of spine density following 24 h application of either control antibody (IgG ab.) or DCC function blocking antibody (DCC ab.). Repeated measure two-way ANOVA, Bonferroni post hoc test, * p < 0.05. Analysis performed on 20 primary dendrites from 5 live neurons per condition over two independent experiments. (**j**) Representative images of fixed dendritic segments, retrogradely labeled with G-deleted rabies-mCherry virus and immunostained with vGAT (inverted fluorescence) and vGLUT1 (inverted fluorescence) antibodies following 24 h application of either control antibody (IgG ab) or DCC function blocking antibody (DCC ab). Scale bar, 10 μm. Density of vGAT and vGLUT1 puncta colocalizing eGFP-filled cell area following 24 h application of either control antibody (IgG ab.) or DCC function blocking antibody (DCC ab.), normalized to vehicle (HBS) controls. N= 9 individual field per condition. The same trend was observed in each of the two independent experiments. Unpaired two-tailed t-test, *p < 0.05. Error bars, SEM.

1047 **Supplemental figures and tables:**

1048 **Figure supplement 1:** Distal axotomy of pyramidal neurons induces dissolution of Nissl
1049 substance without affecting cell viability.

1050 **Figure supplement 2:** Dendrites retract, show fewer branch points and spines 24 h post-
1051 axotomy compared to uninjured controls.

1052 **Figure supplement 3:** FM puncta highly colocalizes with synapsin1 immunolabeling.

1053 **Figure supplement 4:** FM unloading curves from somatodendritic compartments of
1054 microfluidic chambers without rabies virus infection and control conditions

1055 **Figure supplement 5:** RNA quality assessment and verification of microarray quality
1056 controls

1057 **Figure supplement 6:** Fluorescence micrograph of a dually innervated dendritic spine
1058 receiving both excitatory and inhibitory inputs.

1059 **Table supplement 1:** Membrane properties of uninjured controls vs. axotomized neurons
1060 48 h post-axotomy

1061 **Table supplement 2:** List of transcripts that were significantly changed 24 h after injury.

1062 **Table supplement 3**: Cell-cell adhesion transcripts changed 24 h after injury ($p < 0.1$)

1063